

First measurement of the helicity asymmetry  $E$  in  $\eta$  photoproduction on the proton

I. Senderovich<sup>b</sup>, B.T. Morrison<sup>b</sup>, M. Dugger<sup>b</sup>, B.G. Ritchie<sup>b</sup>, E. Pasyuk<sup>b</sup>, R. Tucker<sup>b</sup>, J. Brock<sup>ag</sup>, C. Carlin<sup>ag</sup>, C.D. Keith<sup>ag</sup>, D.G. Meekins<sup>ag</sup>, M.L. Seely<sup>ag</sup>, D. Rönchen<sup>aq</sup>, M. Döring<sup>l,ag</sup>, P. Collins<sup>b,f</sup>, K.P. Adhikari<sup>z</sup>, D. Adikaram<sup>z,1</sup>, Z. Akbar<sup>k</sup>, M.D. Anderson<sup>aj</sup>, S. Anefalos Pereira<sup>o</sup>, R.A. Badui<sup>j</sup>, J. Ball<sup>g</sup>, N.A. Baltzell<sup>a,ae,1</sup>, M. Battaglieri<sup>p</sup>, V. Batourine<sup>ag</sup>, I. Bedlinskiy<sup>t</sup>, A.S. Biselli<sup>i</sup>, S. Boiarinov<sup>ag</sup>, W.J. Briscoe<sup>l</sup>, W.K. Brooks<sup>ah,ag</sup>, V.D. Burkert<sup>ag</sup>, D.S. Carman<sup>ag</sup>, A. Celentano<sup>p</sup>, S. Chandavar<sup>y</sup>, G. Charles<sup>s</sup>, L. Colaneri<sup>q,ac</sup>, P.L. Cole<sup>m</sup>, M. Contalbrigo<sup>n</sup>, O. Cortes<sup>m</sup>, V. Credé<sup>k</sup>, A. D'Angelo<sup>q,ac</sup>, N. Dashyan<sup>an</sup>, R. De Vita<sup>p</sup>, E. De Sanctis<sup>o</sup>, A. Deur<sup>ag</sup>, C. Djalali<sup>ae</sup>, R. Dupre<sup>s</sup>, H. Egiyan<sup>ag,w</sup>, A. El Alaoui<sup>ah</sup>, L. El Fassi<sup>z</sup>, L. Elouadrhiri<sup>ag</sup>, P. Eugenio<sup>k</sup>, G. Fedotov<sup>ae,ad</sup>, S. Fegan<sup>p</sup>, A. Filippi<sup>r</sup>, J.A. Fleming<sup>ai</sup>, A. Fradi<sup>s</sup>, B. Garillon<sup>s</sup>, Y. Ghandilyan<sup>an</sup>, G.P. Gilfoyle<sup>ab</sup>, K.L. Giovanetti<sup>u</sup>, F.X. Girod<sup>ag,g</sup>, D.I. Glazier<sup>aj</sup>, J.T. Goetz<sup>y</sup>, W. Gohn<sup>h,2</sup>, E. Golovatch<sup>ad</sup>, R.W. Gothe<sup>ae</sup>, K.A. Griffioen<sup>am</sup>, M. Guidal<sup>s</sup>, L. Guo<sup>j,ag</sup>, K. Hafidi<sup>a</sup>, H. Hakobyan<sup>ah,an</sup>, C. Hanretty<sup>al,k,1</sup>, M. Hattawy<sup>s</sup>, K. Hicks<sup>y</sup>, D. Ho<sup>e</sup>, M. Holtrop<sup>w</sup>, S.M. Hughes<sup>ai</sup>, Y. Ilieva<sup>ae,l</sup>, D.G. Ireland<sup>aj</sup>, B.S. Ishkhanov<sup>ad</sup>, D. Jenkins<sup>ak</sup>, H. Jiang<sup>ae</sup>, H.S. Jo<sup>s</sup>, K. Joo<sup>h</sup>, S. Joosten<sup>af</sup>, D. Keller<sup>al,y</sup>, G. Khachatryan<sup>an</sup>, M. Khandaker<sup>m,x</sup>, A. Kim<sup>h</sup>, F.J. Klein<sup>f</sup>, V. Kubarovsky<sup>ag</sup>, M.C. Kunkel<sup>ao</sup>, P. Lenisa<sup>n</sup>, K. Livingston<sup>aj</sup>, H.Y. Lu<sup>ae</sup>, I.J.D. MacGregor<sup>aj</sup>, P. Mattione<sup>e</sup>, B. McKinnon<sup>aj</sup>, C.A. Meyer<sup>e</sup>, T. Mineeva<sup>ap</sup>, V. Mokeev<sup>ag,ad</sup>, R.A. Montgomery<sup>o</sup>, A. Movsisyan<sup>n</sup>, C. Munoz Camacho<sup>s</sup>, P. Nadel-Turonski<sup>ag,f,l</sup>, L.A. Net<sup>ae</sup>, S. Nicolai<sup>s</sup>, G. Niculescu<sup>u</sup>, I. Niculescu<sup>u</sup>, M. Osipenko<sup>p</sup>, K. Park<sup>ag,ae,v,3</sup>, S. Park<sup>k</sup>, P. Peng<sup>al</sup>, W. Phelps<sup>j</sup>, S. Pisano<sup>o</sup>, O. Pogorelko<sup>t</sup>, J.W. Price<sup>c</sup>, Y. Prok<sup>z,al</sup>, A.J.R. Puckett<sup>h</sup>, M. Ripani<sup>p</sup>, A. Rizzo<sup>q,ac</sup>, G. Rosner<sup>aj</sup>, P. Roy<sup>k</sup>, F. Sabatié<sup>g</sup>, C. Salgado<sup>x</sup>, D. Schott<sup>l,j</sup>, R.A. Schumacher<sup>e</sup>, E. Seder<sup>h</sup>, A. Simonyan<sup>an</sup>, Iu. Skorodumina<sup>ae,ad</sup>, G.D. Smith<sup>ai</sup>, D.I. Sober<sup>f</sup>, N. Sparveris<sup>af</sup>, S. Stepanyan<sup>ag</sup>, P. Stoler<sup>aa</sup>, I.I. Strakovsky<sup>l</sup>, S. Strauch<sup>ae</sup>, V. Sytnik<sup>ah</sup>, Ye Tian<sup>ae</sup>, M. Ungaro<sup>ag,h</sup>, H. Voskanyan<sup>an</sup>, E. Voutier<sup>s</sup>, N.K. Walford<sup>f</sup>, X. Wei<sup>ag</sup>, M.H. Wood<sup>d,ae</sup>, N. Zachariou<sup>ae</sup>, L. Zana<sup>ai,w</sup>, J. Zhang<sup>ag,z</sup>, Z.W. Zhao<sup>z,ae,ag</sup>, I. Zonta<sup>q,ac</sup>

<sup>a</sup>Argonne National Laboratory, Argonne, Illinois 60439

<sup>b</sup>Arizona State University, Tempe, Arizona 85287-1504

<sup>c</sup>California State University, Dominguez Hills, Carson, CA 90747

<sup>d</sup>Canisius College, Buffalo, NY

<sup>e</sup>Carnegie Mellon University, Pittsburgh, Pennsylvania 15213

<sup>f</sup>Catholic University of America, Washington, D.C. 20064

<sup>g</sup>CEA, Centre de Saclay, Irfu/Service de Physique Nucléaire, 91191 Gif-sur-Yvette, France

<sup>h</sup>University of Connecticut, Storrs, Connecticut 06269

<sup>i</sup>Fairfield University, Fairfield CT 06824

<sup>j</sup>Florida International University, Miami, Florida 33199

<sup>k</sup>Florida State University, Tallahassee, Florida 32306

<sup>l</sup>The George Washington University, Washington, DC 20052

<sup>m</sup>Idaho State University, Pocatello, Idaho 83209

<sup>n</sup>INFN, Sezione di Ferrara, 44100 Ferrara, Italy

<sup>o</sup>INFN, Laboratori Nazionali di Frascati, 00044 Frascati, Italy

<sup>p</sup>INFN, Sezione di Genova, 16146 Genova, Italy

<sup>q</sup>INFN, Sezione di Roma Tor Vergata, 00133 Rome, Italy

<sup>r</sup>INFN, Sezione di Torino, 10125 Torino, Italy

<sup>s</sup>Institut de Physique Nucléaire, CNRS/IN2P3 and Université Paris Sud, Orsay, France

<sup>t</sup>Institute of Theoretical and Experimental Physics, Moscow, 117259, Russia

<sup>u</sup>James Madison University, Harrisonburg, Virginia 22807

<sup>v</sup>Kyungpook National University, Daegu 702-701, Republic of Korea

<sup>w</sup>University of New Hampshire, Durham, New Hampshire 03824-3568

<sup>x</sup>Norfolk State University, Norfolk, Virginia 23504

<sup>y</sup>Ohio University, Athens, Ohio 45701

<sup>z</sup>Old Dominion University, Norfolk, Virginia 23529

<sup>aa</sup>Rensselaer Polytechnic Institute, Troy, New York 12180-3590

<sup>ab</sup>University of Richmond, Richmond, Virginia 23173

<sup>ac</sup>Universita' di Roma Tor Vergata, 00133 Rome Italy

<sup>ad</sup>Skobeltsyn Institute of Nuclear Physics, Lomonosov Moscow State University, 119234 Moscow, Russia

<sup>ae</sup>University of South Carolina, Columbia, South Carolina 29208

<sup>af</sup>Temple University, Philadelphia, PA 19122

<sup>ag</sup>Thomas Jefferson National Accelerator Facility, Newport News, Virginia 23606

<sup>ah</sup>Universidad Técnica Federico Santa María, Casilla 110-V Valparaíso, Chile

Email address: senderov@jlab.org (I. Senderovich)

<sup>1</sup>Current address: Newport News, Virginia 23606

<sup>2</sup>Current address: LEXINGTON, KENTUCKY 40506

<sup>3</sup>Current address: Norfolk, Virginia 23529

<sup>4</sup>Current address: Edinburgh EH9 3JZ, United Kingdom

<sup>ai</sup>Edinburgh University, Edinburgh EH9 3JZ, United Kingdom  
<sup>aj</sup>University of Glasgow, Glasgow G12 8QQ, United Kingdom  
<sup>ak</sup>Virginia Tech, Blacksburg, Virginia 24061-0435  
<sup>al</sup>University of Virginia, Charlottesville, Virginia 22901  
<sup>am</sup>College of William and Mary, Williamsburg, Virginia 23187-8795  
<sup>an</sup>Yerevan Physics Institute, 375036 Yerevan, Armenia  
<sup>ao</sup>Forschungszentrum Jülich, Institut für Kernphysik, 52425 Jülich, Germany  
<sup>ap</sup>University of Waterloo, Institute for Quantum Computing, Waterloo, Ontario, Canada  
<sup>aq</sup>HISKP and BCTP, Universität Bonn, 53115 Bonn, Germany

---

## Abstract

Results are presented for the first measurement of the double-polarization helicity asymmetry  $E$  for the  $\eta$  photoproduction reaction  $\gamma p \rightarrow \eta p$ . Data were obtained using the FROzen Spin Target (FROST) with the CLAS spectrometer in Hall B at Jefferson Lab, covering a range of center-of-mass energy  $W$  from threshold to 2.15 GeV and a large range in center-of-mass polar angle. As an initial application of these data, the results have been incorporated into the Jülich-Bonn model to examine the case for the existence of a narrow  $N^*$  resonance between 1.66 and 1.70 GeV. The addition of these data to the world database results in marked changes in the predictions for the  $E$  observable from that model. Further comparison with several theoretical approaches indicates these data will significantly enhance our understanding of nucleon resonances.

*Keywords:* eta photoproduction; polarization observable; helicity asymmetry

---

## 1. Introduction

Much activity is being devoted to establishing the details of the excitation spectrum of the nucleon in order to deepen our understanding of that fundamental strongly-interacting three-quark system. Due to the broad widths of the nucleon excitations (of the order of 100-300 MeV), the states overlap in the mass spectrum. Thus, disentangling the individual states to identify their exact masses and quantum numbers has been quite difficult. While some resonances are well established, fewer states have been observed than most constituent quark models and Lattice QCD calculations predict [1]. An additional complexity arises because, beyond resonance states with typical widths, approaches based on chiral quark solitons also predict states with far narrower widths than do constituent quark models, including, for example, an  $N_{\frac{1}{2}}^+$  state with a width of 40 MeV or less [2, 3, 4, 5, 6] at about 1.7 GeV; this particular state may have been observed in  $\eta$  photoproduction on the neutron [7, 8, 9].

Since differential cross section measurements alone are insufficient to locate the underlying resonance states or determine their properties, attention has turned to polarization observables. Polarization observables involve interferences between sets of amplitudes, so their measurement can provide stringent tests for predictions of the photoproduction process and help sort out ambiguities in the theoretical description of the reaction in terms the resonances involved. One such polarization observable is the helicity asymmetry  $E$  in pseudoscalar meson photoproduction, which is the normalized difference in photoproduction yield when spins of the incident photon and a longitudinally-polarized target are parallel and anti-parallel.

Formally, this observable is defined as a modulation of the center-of-mass differential cross section  $d\sigma/d\Omega_0$  through the relation

$$\frac{d\sigma}{d\Omega} = \frac{d\sigma}{d\Omega_0} (1 - P_z^T P_\circ^\gamma E), \quad (1)$$

where  $P_z^T$  specifies the degree of longitudinal target polarization and  $P_\circ^\gamma$  is the circular polarization fraction of the incident photon beam. This asymmetry is generally expressed as a function of the center-of-mass energy  $W$  and the polar angle of the produced meson in the center-of-mass frame  $\cos\theta_{cm}$ .

Pion photoproduction studies have contributed greatly to the knowledge of the nucleon resonance spectrum. Recent measurements of spin observables in pion photoproduction [10, 11, 12, 13, 14], have illustrated the power of polarization observables to clarify that spectrum. Even so, many ambiguities still exist and many predicted states remain unobserved. Though pion photoproduction offers a larger cross section, the photoproduction of  $\eta$  mesons exhibits the interesting feature that the process excludes contributions from resonances with isospin  $I = 3/2$ , thereby isolating the  $N^*(I = 1/2)$  states. The  $\eta$  photoproduction process on the proton thus acts as an “isospin filter” for the nucleon resonance spectrum, resulting in a useful tool for disentangling the different states, and is especially important in finding and investigating states that do not couple strongly to pions.

## 2. The Experiment

The measurements reported here are an integral part of a program at Jefferson Lab to achieve a “complete” exper-

iment for the  $\eta$  photoproduction process, whereby all the helicity amplitudes are determined for photoproduction of that pseudoscalar meson. The program began with measurements of the unpolarized differential cross section  $\frac{d\sigma}{d\Omega_0}$  [15, 16] using the large solid angle CEBAF Large Acceptance Spectrometer (CLAS) [17], and the bremsstrahlung photon tagger housed in Jefferson Lab Hall B [18]. For the measurements reported here, circularly polarized photon beams were produced by polarization transfer from the polarized electron beam of the CEBAF accelerator, which was incident on an amorphous radiator of the photon tagger.

The target nucleons for the photoproduction process were free protons in frozen butanol ( $C_4H_9OH$ ) beads inside a 50-mm-long target cup. [19]. The protons of the hydrogen atoms in this material were dynamically polarized along the photon beam direction. The longitudinal target polarization  $P_z^T$  was determined with nuclear magnetic resonance measurements, and averaged  $82 \pm 5\%$ . To minimize systematic uncertainties, the orientation of the target polarization direction was flipped every few days of data-taking between being aligned and anti-aligned with the direction of the incoming photon beam. The helicity of the beam was flipped at a rate of 30 Hz.

Final state particles resulting from photoproduction were detected using CLAS, a set of six identical charged particle detectors installed in a toroidal magnetic field. The principal CLAS subsystems required for this study were the drift chamber systems for tracking charged particles [20], a scintillator-based time-of-flight system [21], and a start counter array which determined when charged particles passed from the target into the detection region [22]. The energy and polarization information for incident photons was provided by the photon tagger.

### 3. Analysis

To determine the helicity asymmetry  $E$  in a discrete event counting experiment, Eq. (1) is inverted to form the asymmetry

$$E = -\frac{1}{|P_z^T||P_e^\gamma|} \left( \frac{N_+ - N_-}{N_+ + N_-} \right), \quad (2)$$

where the detector acceptance cancels. The cross sections are replaced by  $N_+$  and  $N_-$ , which are the number of  $\eta$  mesons counted in beam-target helicity aligned and anti-aligned settings, respectively. The background from non- $\eta$  final states and those from events arising from the unpolarized nucleons within the butanol are subtracted before forming this asymmetry.

Determination of the  $E$  observable requires knowledge of the degree of polarization for both the photon beam and the target proton. The photon beam polarization is calculated from the incident photon energy  $E_\gamma$  relative to the bremsstrahlung endpoint ( $\tilde{E} = E_\gamma/E_{e^-}$ ) via the ex-

pression

$$P_e^\gamma = P_e \frac{4\tilde{E} - \tilde{E}^2}{4 - 4\tilde{E} + 3\tilde{E}^2}, \quad (3)$$

where  $P_e$  is the polarization of the electron beam incident on the amorphous radiator within the photon tagger [23];  $P_e$  was measured with the Hall B Møller polarimeter during the experiment to be  $0.84 \pm 0.01$ .

Events in the detector were reconstructed in the following manner. Individual charged tracks were reconstructed in the CLAS drift chambers and matched to hits in the time-of-flight (TOF) and start counter paddles. The particle identity was determined by combining the information on the momentum of the particle, which was determined by the drift chambers from the curvature of the particle trajectory in the magnetic field, and on the speed of the particle ( $\beta$ ) as determined from the timing information provided by the tagger, start counter, and TOF systems. Charged tracks that could not be reconstructed by all of these detectors were rejected. A track was assumed to have the particle identity that allowed the closest match between the 4-momentum-computed  $\beta$  and the measured value of  $\beta$ . An additional requirement that the measured  $\beta$  was within  $\pm 0.04$  of the expected value was imposed on pion candidates, significantly suppressing the electron background. Once the particle identity was established, a correction due to energy loss in the target and detector materials was performed, with the 4-vector values adjusted accordingly. The tracks and the event as a whole were associated to beam photons based on consistency with the projected vertex timing. To avoid ambiguity, only events with particles matching exactly one beam photon were kept.

The CLAS detector is primarily a charged particle spectrometer, with electromagnetic calorimetry confined to a narrow angular range. Thus,  $\sim 94\%$  of the signal in this analysis relied on missing mass reconstruction of the neutral  $\eta$  from the measured kinematical information of the proton recoiling into the CLAS (the detection of which was required), with the remainder of events having one or both charged pions from the decay  $\eta \rightarrow \pi^+\pi^-\pi^0$  detected. Events with a single detected charged pion were required to have a missing mass squared greater than  $0.06 \text{ GeV}^2/c^4$ , which is the onset of the remaining two-pion phase space. Events with both a  $\pi^+$  and  $\pi^-$  detected were required to have the remaining missing mass squared close to that of the  $\pi^0$  within the detector resolution:  $0.008\text{--}0.028 \text{ GeV}^2/c^4$ .

The  $\eta$  photoproduction data were analyzed to extract the helicity asymmetry  $E$  in 50 MeV-wide center-of-mass energy  $W$  bins and 0.2-wide center-of-mass production  $\eta$  polar angle ( $\cos\theta_{\text{cm}}$ ) bins. Binning in  $W$  begins near the  $\eta$  threshold at 1.5 GeV. These bin widths were chosen to balance between minimizing statistical uncertainties for the extraction while achieving the best energy resolution for the resonance spectrum and most thorough knowledge of the polar distribution of the resonance decay. The analysis procedures described below were performed for each

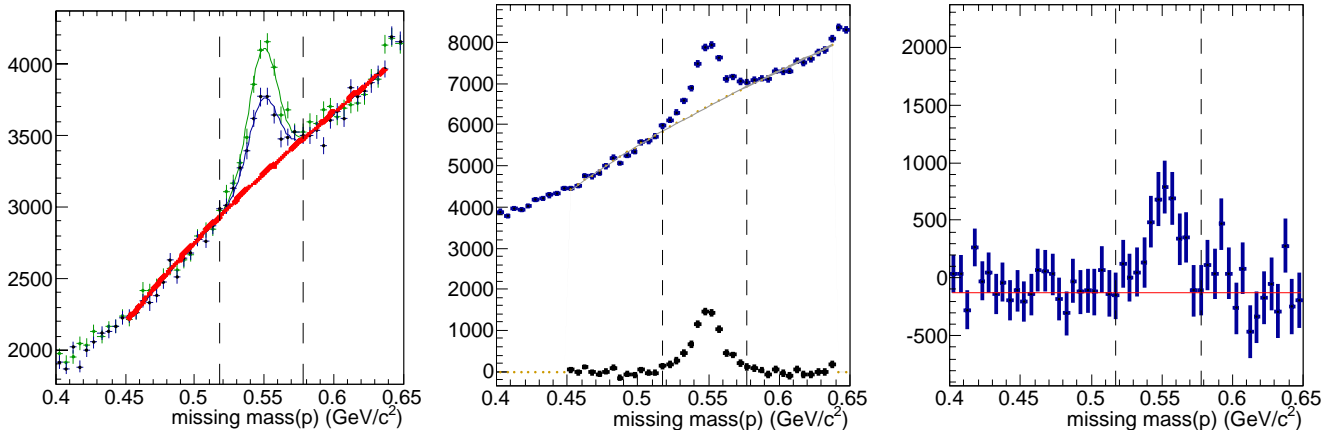


Figure 1: Analysis example for the kinematic bin ( $1650 < W < 1700$  MeV,  $-0.2 < \cos \theta_{\text{cm}} < 0.0$ ). Left panel: Background fit to the missing mass spectra for the two helicities (higher amplitude  $N_-$  is green). Middle panel: Background subtraction and net  $\eta$  yield. Right panel: Yield difference, with fit to sidebands to determine overall asymmetry offset. (Color online)

kinematic bin separately.

To distinguish a photoproduced  $\eta$  from the background, fits were performed to the invariant mass spectra with models of the signal and background included, as shown in Fig. 1. The integral of the fit shape of the background and the uncertainty of this integral from the error matrix estimated the background contribution. Since the detector resolution dominated the shape of the  $\eta$  enhancement, the signal was modeled as a Gaussian. Polynomials were used to model the background, with the order of the polynomial increased progressively with every fit iteration up to fifth order as long as the fit improvement was statistically significant. Specifically, improvement in the confidence level beyond 0.5 was considered not significant. For the two  $W$  bins near the  $\eta$  threshold ( $W < 1.6$  GeV), the step function-like drop-off in photoproduced system phase space required a different approach. For those bins, the error function erf was used in addition to the polynomial, with its amplitude and transition width as free parameters.

A single fit was performed to the spectra of both beam helicities, with a common model of the background shape and common position and width of the  $\eta$  enhancement; an example is shown in the left panel of Fig. 1. The unpolarized background essentially cancels out in the difference of the yield in the missing mass spectra of the two helicities ( $N_+$  and  $N_-$ ) seen in the numerator of Eq. (2); an example is given in the middle panel of Fig. 1. The small remaining overall vertical offset seen for some kinematic bins may be due to asymmetries in the broad polarized background, such as the asymmetry which might exist for the  $\pi^+\pi^-$  final state. These offsets were determined with a fit to the sidebands (as seen in the right panel of Fig. 1), defined as  $\pm 3\sigma$  from the peak center, where the center and  $\sigma$  values were derived from the previously performed fit of the  $\eta$  enhancement. The normalized asymmetry was thus calculated from this corrected difference of helicities divided by the overall  $\eta$  yield determined with the back-

ground subtraction described above.

A separate study of photoproduction on a pure carbon target showed no evidence of peaking in the  $\eta$  mass region. Thus, no correction for the heavier nuclei in the target was required beyond the smooth background fitting described. Helicity asymmetry extraction was not performed when the background exhibited an extremum under the  $\eta$  peak, (*i.e.* within  $\pm 1\sigma$  of the peak centroid) to avoid serious ambiguities between the signal and the background shape. Additionally, analysis in a kinematic bin was abandoned when the total  $\eta$  yield uncertainty was greater than 30%.

Missing mass energy resolution for the  $\eta$  with CLAS is a smooth function of the kinematic space explored here. Therefore, the peak widths seen in the initial independent analyses of the individual kinematic bins were compared and a smooth function of the peak width across the kinematic space was extracted. Yield extractions were then repeated using these constraints on the peak width to enforce consistency with the detector resolution.

Statistical uncertainties dominated the systematic uncertainties in all analyzed bins, and are shown combined in the presented results. The systematic uncertainties include the target polarization  $P_z^T$  uncertainty (6.1%) and photon beam polarization  $P_\gamma^T$  uncertainty (3.1%).

#### 4. Results and discussion

The results for the helicity asymmetry  $E$  are shown in Figs. 2 and 3 for  $1.5 \leq W \leq 2.1$  GeV. At threshold, the  $E$  observable is close to unity due to the dominance of the  $N(1535)\frac{1}{2}^-$  resonance [24], and the results reported here are consistent within uncertainties with this expectation. As  $W$  increases, the presence of other resonances and the interferences of the various amplitudes related to those resonances generate a  $W$ -dependent structure in  $E$ , which models of the production process attempt to describe. As examples of such models, shown in Fig. 2 are predictions

from phenomenological fits by SAID [25], Jülich-Bonn [26] and ANL-Osaka [27].

The figure also shows a new fit with the Jülich-Bonn dynamical coupled-channel approach incorporating the data reported here. In that framework, the hadronic scattering amplitude is constructed with a potential, generated from an effective SU(3) Lagrangian, using time-ordered perturbation theory, and the amplitude is iterated in a Lippmann-Schwinger equation such that unitarity and analyticity are automatically respected.

This new fit also simultaneously incorporated the world databases for the pion-induced production of  $\eta N$ ,  $K\Lambda$  and  $K\Sigma$  final states [28] and the partial-wave solution of the GW/DAC group [29] for elastic  $\pi N$  scattering. It also includes the world data bases of pion and  $\eta$  photoproduction off the proton up to  $W \sim 2.3$  GeV [30, 26], in particular the recent MAMI results on  $T$  and  $F$  in  $\eta$  photoproduction [31].

This new fit also simultaneously incorporated measurements for pion-induced reactions and for pion- and  $\eta$  photoproduction off the proton. The published Jülich-Bonn predictions for  $E$ , as well as this new fit, include the recent MAMI results on  $T$  and  $F$  in  $\eta$  photoproduction

In order to achieve a good fit result, all parameters tied to the resonance states and to the photon interaction had to be modified from the values reported in Ref. [26]. The inclusion of these new  $E$  data also resulted in significant changes in the extracted resonance pole positions. For example, with these new  $E$  data, the  $N(1710)1/2^+$  resonance becomes 45 MeV heavier and 20 MeV wider compared to Ref. [26], with a 40% smaller branching ratio into the  $\eta N$  channel. Helicity couplings for the high-spin  $N(2190)7/2^-$  and  $N(2250)9/2^-$  resonances, whose properties are difficult to determine in general, change their pole positions by up to 80 MeV in the real and 100 MeV in their imaginary parts due to these new  $E$  data.

That the  $E$  data reported here have such a large impact on the resonance parameters might appear surprising. Since the different spin observables have differing combinations of amplitudes, the various observables will have differing degrees of impact on reducing the uncertainties of the parameter values extracted from a fit to the experimental data. In the present case, those parameters are the fundamental electromagnetic properties of resonances, their helicity couplings at the pole.

To study the variations in the statistical impacts on the parameters of the new Jülich fit that arise through the use of measurements of the different spin observables, we have studied the condition number  $\kappa$  for the covariance matrix found in fitting the observed data. The condition number  $\kappa$  is a standard test for diagnosing multicollinearity and, hence, the non-orthogonality of the model parameters on which the fit is based [32]. The condition number  $\kappa$  is defined as  $\lambda_{\max}/\lambda_{\min}$ , that is, the ratio of the largest and smallest eigenvalues. Geometrically,  $\sqrt{\kappa}$  determines the ratio of the longest half-axis of the statistical uncertainty ellipsoid divided by the shortest one. A large  $\kappa$  (say,

greater than 100 [32]) is a sign of moderate to strong multicollinearity, *i.e.* a very elongated statistical uncertainty ellipsoid; larger values of  $\kappa$  thus connote greater uncertainty in the corresponding helicity couplings determined from the fit.

For the present  $E$  data, we found  $\kappa \approx 50$ , while for the other spin observables (and even the differential cross section),  $\kappa$  ranged from 50 to 400. Thus, in terms of minimizing the uncertainties in the extracted parameters, the  $E$  observable measurements reported here indeed turn out to be particularly impactful. This underscores that the observable  $E$  in  $\eta$  photoproduction is especially suited to disentangle electromagnetic resonance properties. With relatively few data points, this measurement offers a larger impact on the baryon spectrum, helicity couplings, and even hadronic decay parameters than might be expected.

Turning next to the putative  $N\frac{1}{2}^+$  resonance near  $W \sim 1.7$  GeV, Fig. 3 shows our results for the observable  $E$  using finer  $W$  bins (of 20 MeV width). Coarser, 0.4-wide binning in  $\cos\theta_{\text{cm}}$  was used to compensate for the narrow energy binning. A fit to this re-binned data using the Jülich-Bonn formalism found that the structure observed at  $\sim 1.7$  GeV for the  $\cos\theta_{\text{cm}}$  bin centered at 0.2 is due to interference between the  $E_0^+$  and  $M_1^+$  multipoles, which vary rapidly at this energy due to the  $N(1650)1/2^-$  and  $N(1720)3/2^+$  resonances. Together with the slowly varying  $E_2^-$  multipole, these three multipoles alone describe the  $E$  asymmetry quite well without the need for an additional narrow resonance near 1.68 GeV. A similar analysis of the multipole content for the  $\cos\theta_{\text{cm}}$  bin centered at  $-0.6$  shows that the interference of the  $E_0^+$  and  $M_2^+$  multipoles (the latter containing the  $N(1675)5/2^-$ ) is responsible for the dip, with  $E_1^+$ ,  $E_2^-$  and  $M_2^-$  necessary to better approximate the full fit. Combined with the hints seen in Refs. [7, 8], the data presented here further motivate additional experimental investigations looking at other spin observables.

In summary, we have presented the first measurements of the helicity asymmetry  $E$  in photoproduction of  $\eta$  mesons from the proton. Initial investigation of these results with the Jülich-Bonn dynamical coupled-channel approach show pronounced changes in the description of this variable when these new data are included, and demonstrate how these measurements are particularly impactful in constraining analyses of the excitation spectrum of the proton. With respect to the existence of an  $N\frac{1}{2}^+$  resonance near  $W \sim 1.7$  GeV suggested previously [2, 3, 4, 5, 6], the data obtained here do not demand the presence of such a state, but further measurements of other polarization observables would be helpful in gaining additional insight on that question.

## Acknowledgements

The authors gratefully acknowledge the work of the Jefferson Lab staff, as well as the support by the National Science Foundation, the JSC(JUROPA) facility at FZ Jülich,

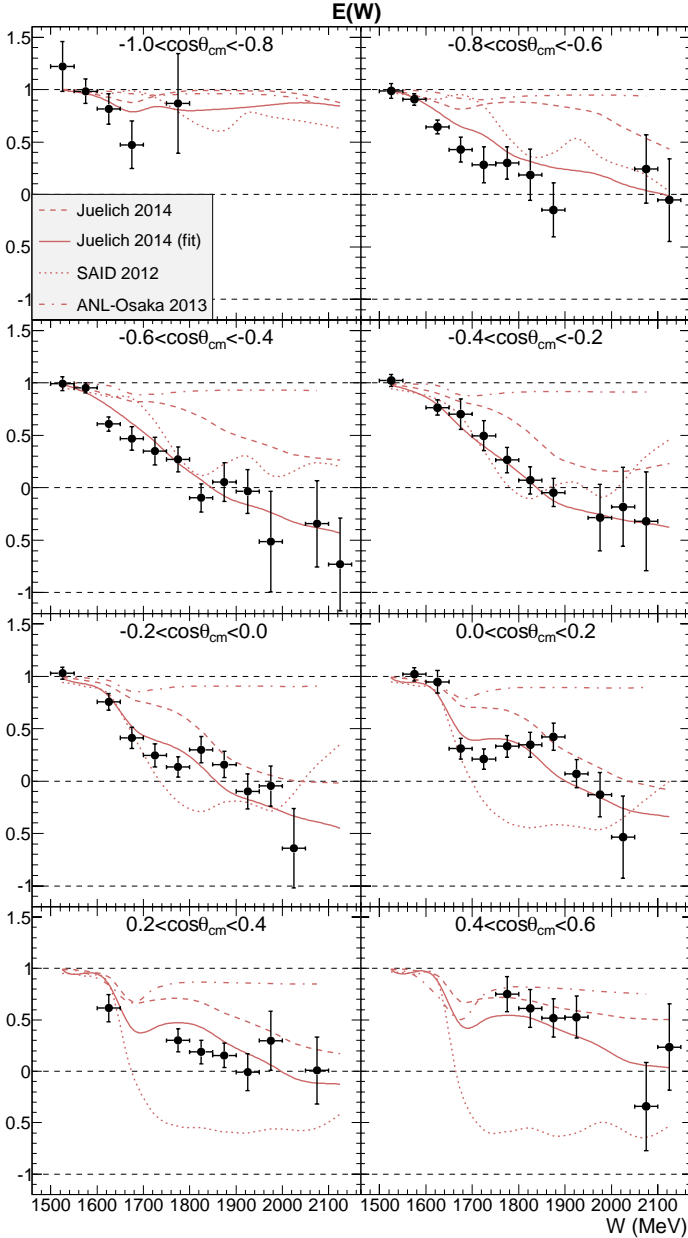


Figure 2: Helicity asymmetry  $E$  for  $\gamma p \rightarrow \eta p$  as a function of  $W$  at various values of  $\cos\theta_{\text{CM}}$  compared to several phenomenological predictions.

the French Centre National de la Recherche Scientifique and Commissariat à l’Energie Atomique, the Italian Istituto Nazionale di Fisica Nucleare, the Chilean Comisión Nacional de Investigación Científica y Tecnológica, the Science and Technology Facilities Council of the United Kingdom, and the National Research Foundation of Korea. This material is based upon work supported by the U.S. Department of Energy, Office of Science, Office of Nuclear Physics under contract DE-AC05-06OR23177.

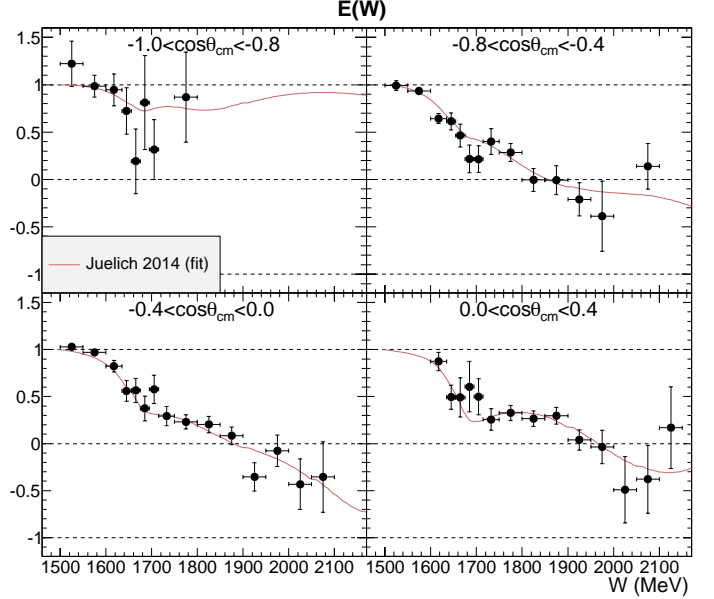


Figure 3: The helicity asymmetry  $E$  for  $\gamma p \rightarrow \eta p$  using smaller  $W$  bins to explore the behavior of the helicity observable near  $W \sim 1.7$  GeV. Predictions of the Jülich-Bonn model as discussed in the text are shown by the solid line.

## References

## References

- [1] E. Klempt, J.-M. Richard, Baryon spectroscopy, *Rev. Mod. Phys.* 82 (2010) 1095–1153.
- [2] D. Diakonov, V. Petrov, M. V. Polyakov, Exotic anti-decuplet of baryons: Prediction from chiral solitons, *Z. Phys.* A359 (1997) 305–314.
- [3] D. Diakonov, V. Petrov, Where are the missing members of the baryon anti-decuplet?, *Phys. Rev.* D69 (2004) 094011.
- [4] R. A. Arndt, Y. I. Azimov, M. V. Polyakov, I. I. Strakovsky, R. L. Workman, Nonstrange and other unitarity partners of the exotic Theta+ baryon, *Phys. Rev.* C69 (2004) 035208.
- [5] J. R. Ellis, M. Karliner, M. Praszalowicz, Chiral soliton predictions for exotic baryons, *JHEP* 0405 (2004) 002.
- [6] M. Praszalowicz, SU(3) breaking in decays of exotic baryons, *Acta Phys. Polon.* B35 (2004) 1625–1642.
- [7] A. V. Anisovich, E. Klempt, V. Kuznetsov, V. A. Nikonov, M. V. Polyakov, et al., *Phys. Lett.* B719 (2013) 89–94.
- [8] D. Werthmüller, et al. (A2 Collaboration), Narrow Structure in the Excitation Function of Photoproduction off the Neutron, *Phys. Rev. Lett.* 111 (2013) 232001.
- [9] V. Kuznetsov, F. Mammoliti, V. Bellini, G. Gervino, F. Ghio, G. Giardina, W. Kim, G. Mandaglio, M. L. Sperduto, C. M. Suter, Evidence for narrow resonant structures at  $W \approx 1.68$  GeV and  $W \approx 1.72$  GeV in real compton scattering off the proton, *Phys. Rev. C* 91 (2015) 042201.
- [10] S. Strauch, et al. (CLAS), Beam-helicity asymmetries in double-charged-pion photoproduction on the proton, *Phys. Rev. Lett.* 95 (2005) 162003.
- [11] M. Gottschall, et al. (CBELSA/TAPS), First measurement of the helicity asymmetry for  $\gamma p \rightarrow p\pi^0$  in the resonance region, *Phys. Rev. Lett.* 112 (2014) 012003.
- [12] D. Krambrich, et al. (Crystal Ball at MAMI, TAPS, A2), Beam-Helicity Asymmetries in Double Pion Photoproduction off the Proton, *Phys. Rev. Lett.* 103 (2009) 052002.
- [13] A. Wilson (CBELSA-TAPS), Helicity beam asymmetry I(sun) in two neutral pseudoscalar photoproduction reactions at the

- Crystal Barrel experiment, AIP Conf. Proc. 1257 (2010) 607–611.
- [14] M. Oberle, et al. (MAMI, TAPS, A2), Measurement of the beam-helicity asymmetry  $T^{\odot}$  in the photoproduction of  $\pi^0\pi^{\pm}$  pairs off protons and off neutrons, Eur. Phys. J. A50 (2014) 54.
- [15] M. Dugger, et al. (CLAS Collaboration), Eta photoproduction on the proton for photon energies from 0.75 GeV to 1.95 GeV, Phys. Rev. Lett. 89 (2002) 222002.
- [16] M. Williams, et al. (CLAS Collaboration), Differential cross sections for the reactions  $\gamma p \rightarrow p\eta$  and  $\gamma p \rightarrow p\eta'$ , Phys. Rev. C80 (2009) 045213.
- [17] B. A. Mecking, et al. (CLAS), The CEBAF Large Acceptance Spectrometer (CLAS), Nucl. Instrum. Meth. A503 (2003) 513–553.
- [18] D. I. Sober, H. Crannell, A. Longhi, S. K. Matthews, J. T. O'Brien, et al., The bremsstrahlung tagged photon beam in Hall B at JLab, Nucl. Instrum. Meth. A440 (2000) 263–284.
- [19] C. Keith, J. Brock, C. Carlin, S. Comer, D. Kashy, et al., The Jefferson Lab Frozen Spin Target, Nucl. Instrum. Meth. A684 (2012) 27–35.
- [20] M. D. Mestayer, D. S. Carman, B. Asavapibhop, F. J. Barbosa, P. Bonneau, et al., The CLAS drift chamber system, Nucl. Instrum. Meth. A449 (2000) 81–111.
- [21] E. S. Smith, T. Carstens, J. Distelbrink, M. Eckhause, H. Eghian, et al., The time-of-flight system for CLAS, Nucl. Instrum. Meth. A432 (1999) 265–298.
- [22] Y. G. Sharabian, M. Battaglieri, V. D. Burkert, R. De Vita, L. Elouadrhiri, et al., A new highly segmented start counter for the CLAS detector, Nucl. Instrum. Meth. A556 (2006) 246–258.
- [23] H. Olsen, L. C. Maximon, Photon and Electron Polarization in High-Energy Bremsstrahlung and Pair Production with Screening, Phys. Rev. 114 (1959) 887–904.
- [24] V. Hejny, P. Achenbach, J. Ahrens, R. Beck, S. Hall, et al., Near threshold photoproduction of eta mesons from He-4, Eur. Phys. J. A6 (1999) 83–89.
- [25] E. McNicoll, et al. (Crystal Ball at MAMI), Study of the  $\gamma p \rightarrow \eta p$  reaction with the Crystal Ball detector at the Mainz Microtron(MAMI-C), Phys.Rev. C82 (2010) 035208.
- [26] D. Rönchen, M. Döring, H. Haberzettl, J. Haidenbauer, U. G. Meißner, et al., Eta photoproduction in a combined analysis of pion- and photon-induced reactions, Eur. Phys. J. A51 (2015) 70.
- [27] H. Kamano, S. X. Nakamura, T. S. H. Lee, T. Sato, Nucleon resonances within a dynamical coupled-channels model of  $\pi N$  and  $\gamma N$  reactions, Phys. Rev. C88 (2013) 035209.
- [28] D. Rönchen, M. Döring, F. Huang, H. Haberzettl, J. Haidenbauer, C. Hanhart, S. Krewald, U. G. Meißner, K. Nakayama, Coupled-channel dynamics in the reactions  $\pi N \rightarrow \pi N$ ,  $\eta N$ ,  $K\Lambda$ ,  $K\Sigma$ , Eur. Phys. J. A49 (2013) 44.
- [29] R. L. Workman, R. A. Arndt, W. J. Briscoe, M. W. Paris, I. I. Strakovsky, Parameterization dependence of T matrix poles and eigenphases from a fit to  $\pi N$  elastic scattering data, Phys. Rev. C86 (2012) 035202.
- [30] D. Rönchen, M. Döring, F. Huang, H. Haberzettl, J. Haidenbauer, C. Hanhart, S. Krewald, U. G. Meißner, K. Nakayama, Photocouplings at the Pole from Pion Photoproduction, Eur. Phys. J. A50 (2014) 101. [Erratum: Eur. Phys. J.A51,no.5,63(2015)].
- [31] C. S. Akondi, et al. (A2 at MAMI), Measurement of the Transverse Target and Beam-Target Asymmetries in  $\eta$  Meson Photoproduction at MAMI, Phys. Rev. Lett. 113 (2014) 102001.
- [32] D. C. Montgomery, E. A. Peck, G. G. Vining, Introduction to linear regression analysis (2012) 298.